Tuning the extent of porosity and composition of N-doped carbon materials by $NaNO_3$ and its effect on electrochemical activity

Yimai Chen[a], Hui Wang[a], Shan Ji[b,*], Bruno G. Pollet[c] and Rongfang Wang[a,**]

[a] Institute of Chemical Engineering, Qingdao University of Science and Technology, Qingdao, 266042, China

[b] College of Biological, Chemical Science and Chemical Engineering, Jiaxing University, Jiaxing, 314001, China

[c] Department of Energy and Process Engineering, Faculty of Engineering, Norwegian University of Science and Technology (NTNU), NO-7491 Trondheim, Norway

Corresponding authors:

Shan Ji (*): jissshan@126.com, Tel./fax: +86 (0)15024355548

Rongfang Wang (**): wrf38745779@126.com, Tel./fax: +86 (0)13919839172

Abstract: A facile one-pot method using $NaNO_3$ as etching agent in a molten salt medium is developed to tune the porous structure and composition of N-doped carbon materials derived from biomass at high temperatures. SEM and TEM analyses reveal that by increasing the amount of $NaNO_3$, the structures of the obtained carbons become more open and graphene-like layers are formed. N_2 adsorption/desorption isotherms show that the hierarchical porous structure could be efficiently tuned by adjusting the amount of $NaNO_3$ in the salt mixture. It is observed that the specific

surface area of the as-prepared N-doped carbon using $NaNO_3$ can reach 1,430.1 $m^2 g^{-1}$, a much higher value than that of the sample prepared in the absence of $NaNO_3$. The micropore ratio decreases with increased amount of $NaNO_3$, from 49.42 % to 9.98 %. Whilst the surface composition of the obtained carbon materials is affected by $NaNO_3$. The N content increases and O decreases respectively, by increasing the amount of $NaNO_3$. Analysis on the N 1*s* high resolution reveals that the sum of pyridinic-N and graphitic-N increased, whereas the sum of pyridinic-N oxide and NO_x decreases from NC-0 to NC-0.75. It is also found that the changes of the porous structure and the oxygen-containing groups from NC-0 to NC-0.75 led to changes in hydrophilicity. When the as-prepared carbon materials are used as catalysts for the oxygen reduction reaction, high catalytic activity values are obtained, sample NC-0.5 shows the best performance due to the porous structure and doping effect of N atoms. More importantly, it is concluded that producing N-doped carbon materials from soybean dregs in molten salt medium using $NaNO_3$ as etching agent could provide a promising approach for the synthesis of opened N-doped carbons of controlled porous structures and large specific surface areas based on biomass precursors.

Keywords: N-doped carbon; $NaNO_3$; Controlled porous structure; Catalysis; Capacitance.

1. Introduction

Porous carbon materials, especially those with targeted functionalities, i.e. the

broad range of heteroatom-containing porous carbons possessing high specific surface areas (apparent surface area > 1,000 m^2 g^{-1}), are one of the most competitive material choices in many applications such as catalysis and water treatment, when compared to other classes of porous materials such as zeolites, porous silica, MOFs and many others [1, 2]. This is due to their "lightweight constructions" (with each "module" just weighting 12 mass units), but also due to the extraordinary chemical, mechanical and thermal stability of carbon materials and their wide abundance [3].

To produce such materials of adequate porosity, it is often necessary to use hard and soft templating techniques [4, 5]. In the hard-templating strategy, porous materials such as zeolite or porous silica with definite-sized pores are often used as porogen to form the pores in the carbon structure [6-9]. Although porous structures of high surface areas can be obtained, two crucial steps during the preparation are required; the first step, hard templating, involves the synthesis and removal of the crystalline template afterwards, making such a process barely scalable [10]. In the case of soft templating, a large number of surfactants or/and organic polymers such as organic polymers acting as the template to form the porous structure is used [11-15]. Most of these reagents are hazardous and costly chemicals. The soft templating method is not an economic and "green" method for the synthesis of porous carbon materials. Another way for the synthesis of carbon materials of desired porosity is the chemical activation method. In this chemical activation process, the pores are etched into the carbon material by the chemical reaction between the etching agents (e.g. an alkali hydroxide or a stream of CO_2) and carbon [16-18]. This method has been

successfully employed to produce porous carbon materials at industrial scale owing to its simplicity. Nonetheless, improvement of the chemical activation technique for the rational pore design is still required, for example reducing the carbon mass loss and minimizing the chemical composition changes in regard to the dopants (e.g. structural nitrogen).

In the jewelry industry, $NaNO_3$ has been used as etching agent to mechano-chemically super-polish diamond surfaces as decomposed oxygen from $NaNO_3$ can chemisorb on the surface and react with carbon to form CO and CO_2 [19]. This observation implies that $NaNO_3$ could act as chemical active agent for producing porous carbon materials. Moreover, a few studies have reported that the use of nitrates such as $LiNO_3$ and $Co(NO_3)_2$ as chemical activation agents leads to the generation of the pores in the carbonaceous material structure [20]. Compared with $LiNO_3$ and $Co(NO_3)_2$, $NaNO_3$ is much cheaper and mild etching agent. Therefore, in this study, $NaNO_3$ was used with $NaCl/ZnCl_2$ to form eutectic molten salt during the carbonization process of SD, in the hope of using less salt to prepare porous nitrogen-doped (N-doped) carbon materials with tunable porous structures. Furthermore, the extent of the porosity development and corresponding pore size distribution of the obtained N-doped materials can be tuned by carefully controlling the amount of $NaNO_3$ in the process. The physical results showed that the presence of $NaNO_3$ had a substantial impact on the thickness of the carbon sheets, mesoporous structure and specific surface area of the N-doped carbon materials, in turns affecting their electrochemical performance. Compared with reported $LiNO_3$ method, $NaNO_3$

etching process resulted in more fluffy carbon network, of which the specific surface area and total pore volume are larger, when consuming the same quantity of etching agents [20]. In our investigation, it was found that these as-prepared materials exhibited large capacitance and acceptable ORR activity values (*on-par* with those obtained for commercial Pt/C materials).

2. Experimental

2.1 Preparation of SD-derived mesoporous N-doped carbons

The detailed procedure for preparing mesoporous N-doped carbons derived from soybean dregs (SD) is as follows: SD was first dried at 80 °C in oven for 4 days, and then the dried SD was sifted through a 80 mesh sieve to remove large particles. 1 g of dried SD was mixed with 10 g NaCl/$ZnCl_2$ (NaCl 80 mol%) mixture and *x* g of $NaNO_3$ (which is acted as oxidizing agent to publish the surface of obtained carbon materials at high temperature), then ball milled in a zircon jar at 600 rpm for 6 hours. After that, the mixture was loaded into a ceramic crucible and then placed in an inert gas tube furnace. The temperature was increased to 900 ^oC with a heating rate of 2.5 ^oC min^{-1} under nitrogen atmosphere, and kept at this temperature for 60 mins. Subsequently, the temperature was cooled down to 50 ^oC at a cooling rate of 5 ^oC min^{-1}. The obtained product was immersed into 400 ml of H_2O (ultrapure) and magnetically stirred for 6 h, filtered out and then dried at 80 °C in a vacuum oven for 12 h. Afterwards, the carbon material was immersed in 2 M HNO_3 solution for 24 h to remove inorganic insoluble components, if any. After acid washing, the sample was

washed with ultrapure water until the pH of the filtered water reached neutrality, and then dried at 80 °C in a vacuum oven for 12 h again. The final N-doped carbons were labeled as NC-*x* (*x* is the mass of $NaNO_3$ in the mixed salts). For comparison purposes, a sample made of SD mixed with 10 g of NaCl/$ZnCl_2$ mixed salts without $NaNO_3$ was also prepared by the same method for preparing NC-*x*. The final product was labeled as NC-0.

2.2 Physical characterizations

X-ray diffraction (XRD) patterns were performed on a Shimadzu XD–3A with CuKα radiation. The scans were conducted between 5° to 80° with a rate 4° min^{-1} for 2θ values. The morphology of the carbon samples was studied by scanning electron microscopy (SEM) and transmission electron microscopy (TEM). The SEM images were generated on a Carl Zeiss Ultra Plus. TEM images of the catalysts were conducted on a JEOL (JEM-2000 FX) microscope operating at 200 kV. Specific surface areas were determined by the nitrogen (N) adsorption region of relative pressures from 0.05 to 0.25, and the total pore volume was measured at 0.99. Furthermore, the pore size distribution was obtained using the density functional theory (DFT) method. X-ray photoelectron spectroscopy (XPS) spectra were generated with a PHI-5702 multifunctional X-ray photoelectron spectrometer (American). Binding energies were calibrated by referencing to the C 1*s* peak at 285.0 eV. Water contact angles were measured using an SL200KB apparatus at ambient temperature. For all measurements, the volume of water was 5 μ L. Raman spectroscopy was recorded on a FT-Raman spectrometer (RFS 100, BRU-KER) with

a 1,064 nm excitation laser beam wavelength. The intensity of *D* and *G* peaks was gauged by the height from the top point of each band.

2.3. Electrochemical characterizations

The electrochemical activities were performed using a potentiostat/galvanostat CHI650D (CH Instruments). A rotating disc glass carbon (GC) electrode of diameter 5 mm was used as the working electrode, a Pt wire as the counter electrode and a Ag/AgCl (saturated KCl) as the reference electrode. The GC disc electrode was carefully polished and cleaned before and after each test. Each carbon suspension slurry was prepared by making 2 mg of activated carbon dispersed in 0.4 mL Nafion®/ethanol (0.25% Nafion®) solution. After ultrasonication (ultrasonic bath, 38 kHz) for 20 min, 10 μL of the catalyst ink was applied onto the GC disc electrode, and then dried at room temperature. The geometric area of the working electrode was about 0.196 cm^2, and the mass loading of each carbon materials as well as commercial 20 wt.% Pt/C was about 0.255 mg cm^{-2}. Through careful calculation, the Pt-loading on the disc electrode was approximately 51 μg_{Pt} cm^{-2}.

3. Results and discussion

During the chemical activation process, the formation of pores is accompanied by a mass loss resulting from the reaction between the etching agent and carbon. The effect of $NaNO_3$ on the yield of the final carbon materials is shown in Fig. 1. It is clearly observed from the photographs that the yield of the final carbon materials decreases with increasing amount of $NaNO_3$. When the $NaNO_3$ mass relative to the SD

precursor increases from 0.25 to 0.75, the carbon material yields (relative to the precursor) decreases from 22.7% to 17.0%. This carbon mass loss can be explained as follows: during the carbonization process, high temperatures are used and the $NaNO_3$ etching agent decomposes in turns generating O_2, which is absorbed on the carbonized SD; subsequently the reaction between O_2 and the carbon occurs with the formation of CO and CO_2, leading to the loss of carbon. This observation suggests that the effect of $NaNO_3$ on the structure of the carbon materials requires to be studied in detail to avoid excessive usage of $NaNO_3$.

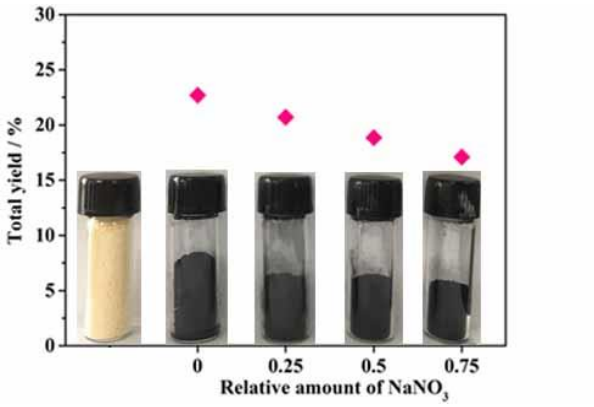

Fig. 1. From left to right, photographs of the SD precursor sample and the obtained carbon material samples, as well as the yield of final carbon materials *vs.* the amount of $NaNO_3$ relative to the SD precursor.

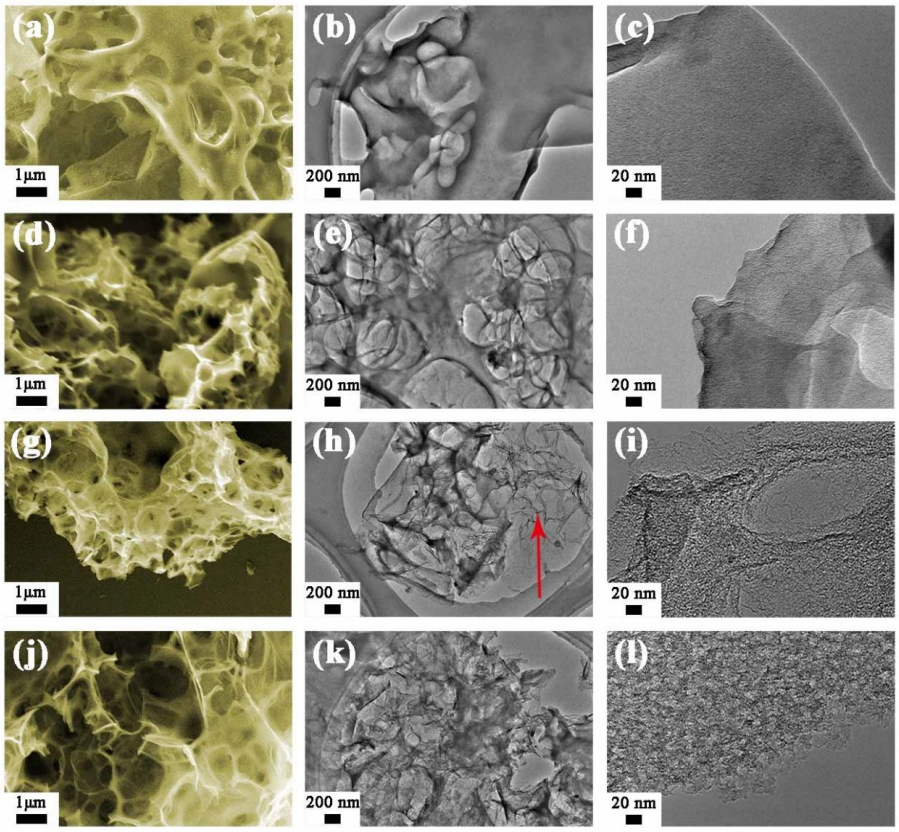

Fig. 2. SEM pictures of (a) NC-0, (d) NC-0.25, (g) NC-0.5, and (j) NC-0.75 samples; and TEM pictures of (b,c) NC-0, (e,f) NC-0.25, (h,i) NC-0.5, and (k,l) NC-0.75 samples.

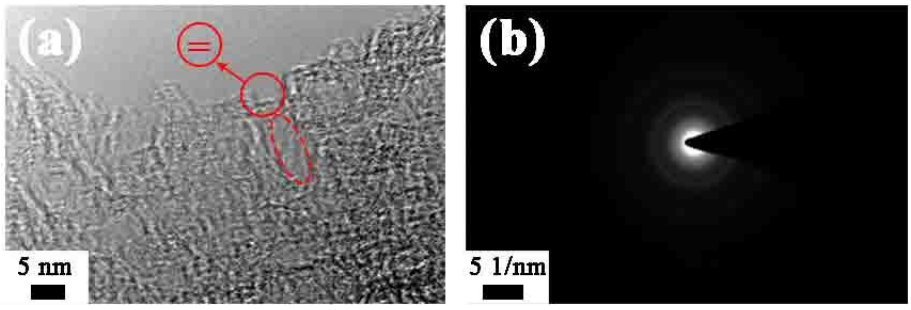

Fig. 3. (a) High resolution TEM and (b) the electron diffraction of catalyst NC-0.5.

The morphology and fine structure of the as-prepared N-doped carbon materials of various amounts of $NaNO_3$ were characterized by SEM and TEM as shown in Fig. 2. As shown in Fig. 2(a), NC-0 presents sponge-like morphology with an open structure.

TEM image in Fig. 2(b) displays an open structure made of interconnected macropores. When $NaNO_3$ was introduced into the salt mixture, the obtained NC-0.25 (Fig. 2(e, f)) exhibited a much open morphology compared to that of NC-0, and the walls became thin and comparable to those observed for NC-0. These changes were mainly due to the etching effect of $NaNO_3$. When the amount of $NaNO_3$ was increased to 0.5 g, the etching effect was further pronounced, which led to NC-0.5 possessing a more open morphology with thinner walls as shown in Fig. 2(h). Moreover as shown in the TEM image in Fig. 2(h), graphene-like carbon layers (indicated by the red arrow) were observed, confirming that the $NaNO_3$ could etch these thick walls at high temperatures. To get more detail information of the graphene-like layer for NC-0.5, high resolution TEM was also conducted and presented in Fig. 3(a). As indicated by the red circle, the pore wall is mainly composed of two layers, in corresponding to above graphene-like structure. While the electron diffraction of NC-0.5 in Fig. 3(b) shows foggy pattern surrounded by haloes, suggesting the presence of defects in the graphene-like architecture, since the carbonization temperature was high enough. It can also be observed that the open structure does not obviously change from the SEM and TEM images, as shown in Fig. 2(j,k), as the amount of $NaNO_3$ is increased to 0.75 g, suggesting that this amount of $NaNO_3$ is sufficient for optimizing the open structure of the obtained carbon materials. For further observations of the microstructural changes of these carbon materials, the enlarged TEM images are presented in Fig. 2 (c, f, i and l). From Fig. 2(c) and (f), a few bright spots with mesoporous size can be observed. For the case of NC-0.5 (Fig.

2(i)) and NC-0.75 (Fig. 2(l)), many mesopores can be observed, suggesting that the amount of mesopores increases with increasing $NaNO_3$. The change in appearance confirms that $NaNO_3$ can reach the inner structure of the carbon to etch, then in turn expanding the size of the pores. It is expected that the obtained open structure and mesopores could provide more accessible active surface area in contact with the electrolyte and facilitate mass diffusion between the electrolyte and the active materials, leading to enhanced electrochemical performance.

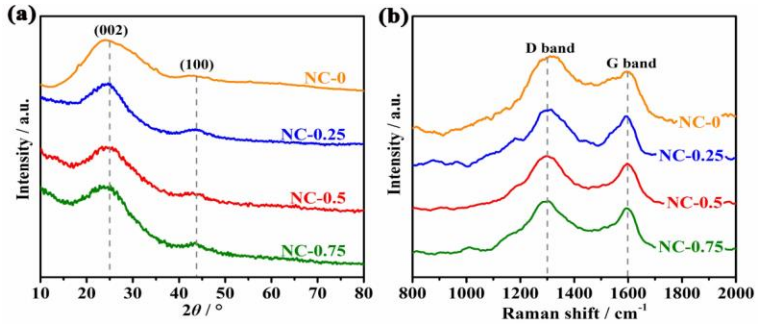

Fig. 4. XRD patterns and Raman spectra of the as-prepared samples.

Fig. 4(a) shows the X-ray diffraction (XRD) patterns of the as-prepared samples. All XRD patterns a) show two diffraction peaks at 2θ values of ca. 25° as well as 43° and b) are similar to that of graphite [21], but the two peaks at ca. 25° as well as 43° are broad suggesting that the graphitization of all the as-prepared samples was weak. All these carbon materials were heated at relatively low temperatures i.e. at 800 °C, which could be the reason why the graphitization was ineffective. The low degree of graphitization implies that the as-obtained carbon materials led to partially disordered structures. By comparison, there is no obvious shifts of the peak position in the four curves, indicating close graphitization degree among the four carbon samples. It can

thus be concluded that $NaNO_3$ made little influence on the graphitization degree of the final material. The disordered structure of these samples was further investigated by Raman spectroscopy (Fig. 4(b)). All Raman spectra exhibited two peaks, namely *D*-band at ca. 1,301 cm^{-1} and 1,600 cm^{-1}. *D*-band arises from structural defects and partially disordered structures, and the *G*-band from an ideal graphitic lattice vibrations of sp^2-bonded carbon atoms [22]. The ratio of I_D/I_G is indicative of the crystallinity of carbon, namely lower I_D/I_G means higher crystallinity [21, 23, 24]. The I_D/I_G for the NC-0, NC-0.25, NC-0.5, and NC-0.75 samples were found to be 1.097, 1.114, 1.125, and 1.151 respectively. It can be seen that the I_D/I_G of samples increases with increasing amount of $NaNO_3$, implying the presence of edges and defects in the obtained carbon samples as more $NaNO_3$ was introduced into the carbonization process, which is in good agreement with the SEM and TEM results.

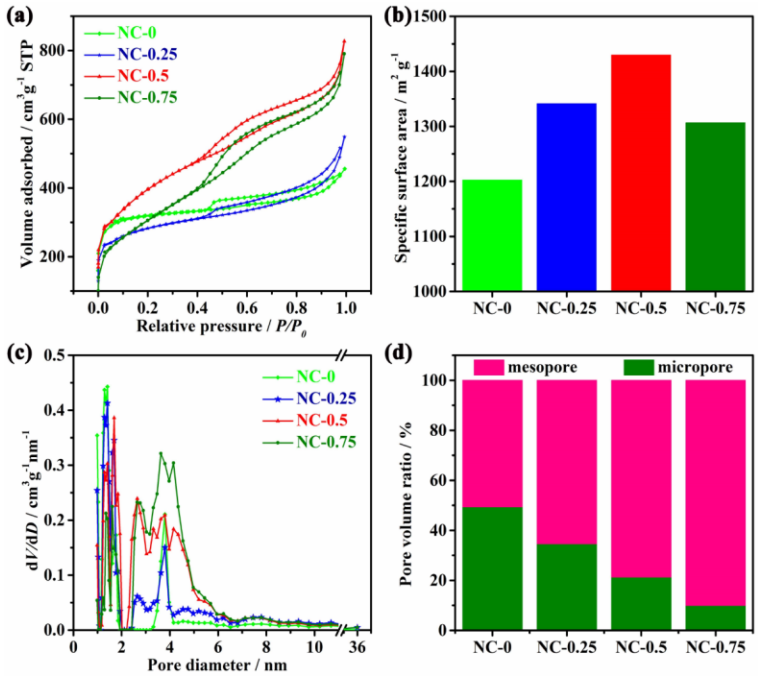

Fig. 5. (a) N_2 adsorption-desorption isotherms, (b) BET surface area, (c) Pore size

distribution and (d) pore volume ratio of mesopore / micropore of the four samples.

To further investigate the effect of $NaNO_3$ on the porous structure of the as-prepared N-doped carbon materials obtained from various amounts of $NaNO_3$, the nitrogen isotherm method was employed to study the porous structures of these materials (Fig. 5(a)). According to *IUPAC* classification, all obtained N_2 isotherms of NC-0, NC-0.25, NC-0.5 and NC-0.75 belonged to mixed types, namely *type I* at relative low pressures and *type IV* at relative intermediate to high pressures [25]. All these isotherms show an obvious uptake in the initial part, which is characteristic of micropores[26]. In these four isotherms, at the relative intermediate and high pressure, hysteresis slopes were observed, indicating the existence of mesopores, especially, for NC-0.5 and NC-0.75 samples; the hysteresis slopes were very obvious and accompanied with rapid N_2 uptake at relative high pressures, indicating the existence of macropores. This finding suggests that these two samples could act as buffer for storing electrolyte whilst facilitating mass diffusion [20]. Based on these adsorption curve of N_2 isotherms, the specific surface areas of the four samples were calculated using the Brunauer-Emmett-Teller (BET) model and plotted as shown in Fig. 5(b). The specific surface area of NC-0 was found to be 1,202.7 $m^2 g^{-1}$, which increased to 1,341.4 $m^2 g^{-1}$ for NC-0.25 after $NaNO_3$ was used as etching agent. The surface area increased to 1,430.1 $m^2 g^{-1}$ as the $NaNO_3$ amount was 0.5 g, however, it decreased to 1,306.8 $m^2 g^{-1}$ for the NC-0.75 sample. The increase in the surface area from 1,202.7 $m^2 g^{-1}$ to 1,430.1 $m^2 g^{-1}$ was due to an ever more open structure, which was confirmed by the SEM images and the formation of many mesopores, confirmed by the TEM

images. As presented in the SEM image for NC-0.75, large amount of $NaNO_3$ may hinder the "opening" of the carbon structure, resulting in no changes in the surface area.

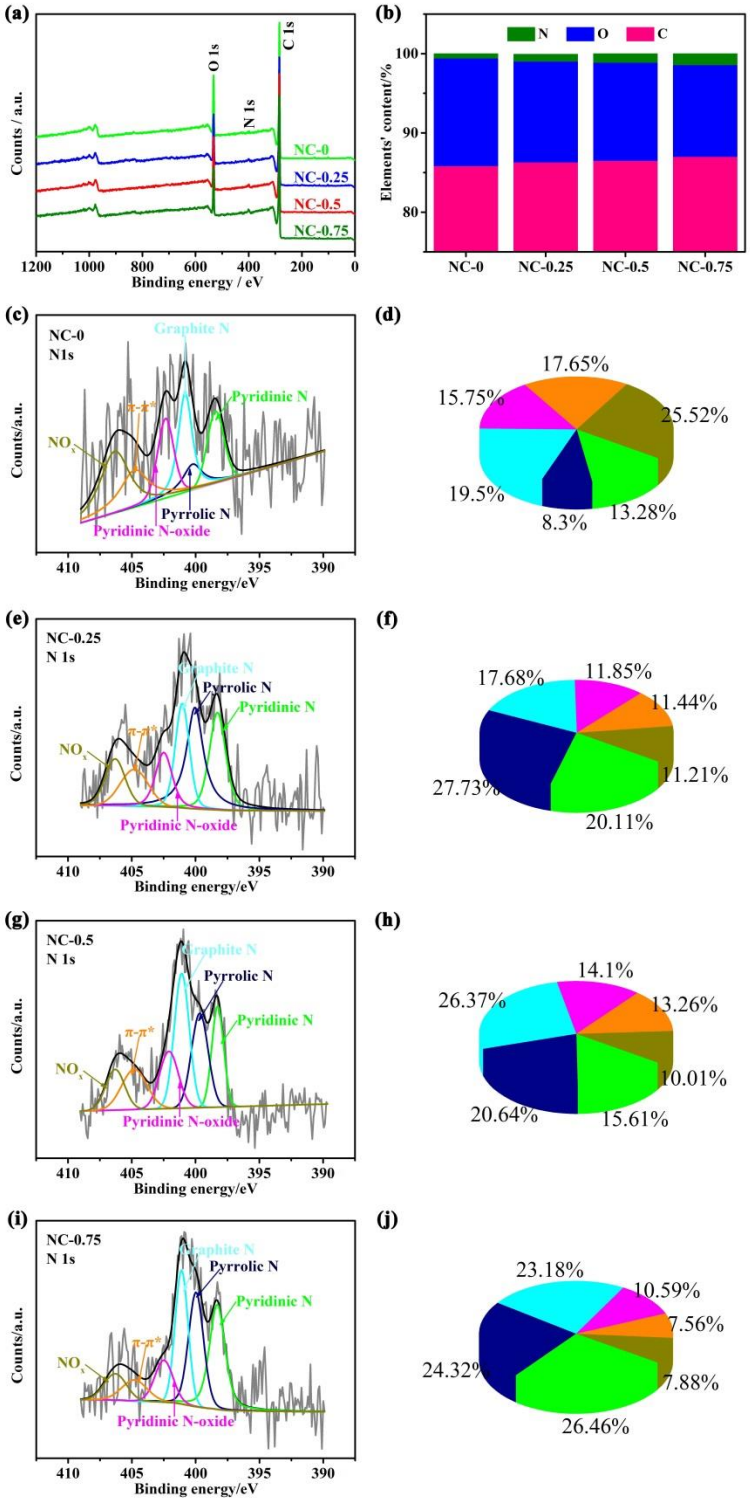

Fig. 6. (a) XPS full spectra of the four samples; (b) the surface composition of the

four samples; The high resolution scans of N 1*s* and each chemical type content for N 1*s* for NC-0 (c, d), NC-0.25(e, f), NC-0.5(g, h), and NC-0.75(i, j).

The pore size distribution of the four samples is shown in Fig. 5(c). In the case of NC-0, it can be observed that there is co-existence of micropores and mesopores, and the micropores make up ca. 60% of the total porosity (Fig. 5(d)). When $NaNO_3$ was introduced, the mesopores, for example in NC-0.25, increased and the proportion of the micropores decreased to 55%, accounting for the increase in the BET surface area. This finding can also be observed for NC-0.5 and NC-0.75 when the amount of $NaNO_3$ is increased. These changes indicate that the pores in the carbon material structure become larger as some carbon site was etched by $NaNO_3$. In addition, the etching effect of $NaNO_3$ resulted in an increase of the total pore volume from 0.705 $cm^3\ g^{-1}$ for NC-0 to 0.949 $cm^3\ g^{-1}$ for NC-0.25, to 1.379 $cm^3\ g^{-1}$ for NC-0.5 and to 1.323 $cm^3\ g^{-1}$ for NC-0.75. It was recently reported that the mesopores can facilitate the ionic transportation in the porous materials and improve the ionic diffusion kinetics, resulting in an enhanced electrochemical performance . Therefore, it may be expected that the NC-0.5 and NC-0.75 samples containing larger amount of mesopore could yield better electrochemical behaviours than others.

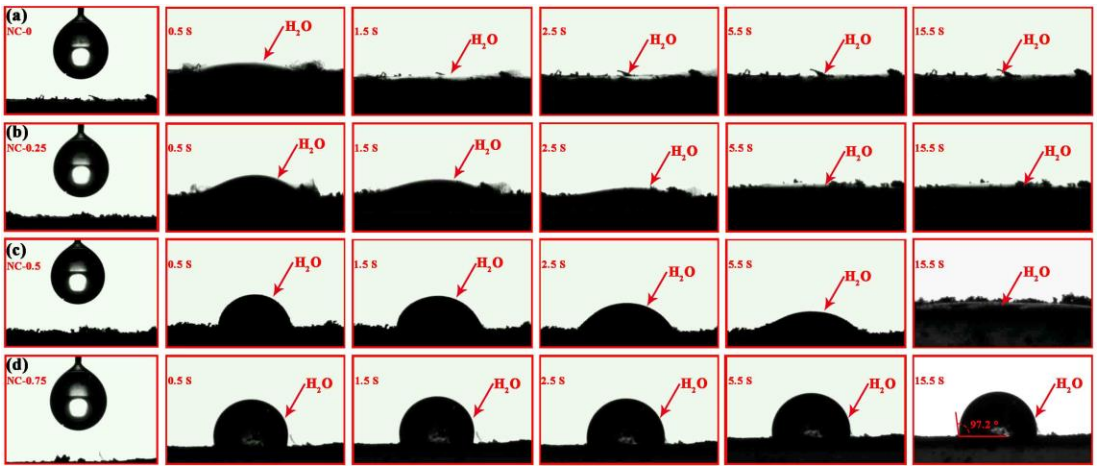

Fig. 7. The speeding process of a droplet on (a) NC-0, (b) NC-0.25, (c) NC-0.5, and (d) NC-0.75 carbon materials.

The effect of $NaNO_3$ on the sample surface composition (within a range of 0.1-10 nm) and elemental chemical state, was investigated by X-ray photoelectron spectroscopy (XPS) (Fig. 6). From the figure, it can be observed that clear signals of N 1*s*, C 1*s* and O 1*s* are visible in the spectra of the four samples (Fig. 6(a)), indicating that the obtained carbon materials are mainly made of C, N and O elements. On the other side, the faint signals centered around 200.0 eV should a symbol of Cl for above four samples. However, there is no obvious Na signal, because of its easy washing out in the open porosity, just like K and Li elements. Even if there is any auger Zn one, it should be covered up by O loss one. It can be concluded that there might be trace amount of $ZnCl_2$ trapped in closed pores. However, the electrochemical performance affected by Zn can be neglected [27]. It can also be observed that the signal of N 1*s* becomes stronger from NC-0 to NC-0.75, indicating that the N content increases. Fig. 6(b) shows the atom ratio of the elements in the surface. It can be seen that the N content increases, indicating that the surface

composition of the obtained carbon materials changes with increased amount of $NaNO_3$. Moreover, the O content decreased from NC-0 to NC-0.75, indicating that the amount of the oxygen-containing functional group decreased with increased $NaNO_3$.

To outsight the chemical state of N atoms, the N 1*s* high resolution spectra for all the samples were fitted. Fig. 6(c-j) shows that the presence of six types of nitrogen species on all the sample surfaces, namely, pyridinic-N at 397.8 eV, pyrrolic-N at 399.4 eV, graphitic-N at 401.0 eV, pyridinic N-oxide at 401.9 eV, π-π* satellite at 404.8 eV, and entrapped NO_x at 406.3 eV [28]. Detailed percentage of these N species in all the samples are also illustrated in Fig. 6. The sum of graphitic-N and pyridinic-N increased from NC-0 to NC-0.75. It was recently demonstrated that graphitic-N and pyridinic-N materials are active toward the oxygen reduction reaction (ORR) [29-31]. This indicates that a better ORR performance should be obtained for the NC-0 to NC-0.75 samples. It was also found that the percentage of the oxidized N atoms present in the pyridinic N-oxide and entrapped NO_x decreased as the amount of $NaNO_3$ was increased. The amount of N atoms with richer electron decreased, leading to a weak interaction between N atom and H atom in water molecule, and therefore resulting in a decrease in the hydrophilic property. To prove this change, water contact angle tests were performed. As illustrated in Fig. 7(a), the water droplet spreads out on NC-0 within 1.5 s and adsorbed immediately in the following 4 s through capillary forces, resulting in 0° contact angle. This wetting behaviour toward water is due to microscale rough surface as well as abundant hydrophilic groups [32]. In contrast, on NC-0.25 (Fig. 7(b)), the droplet spreading process happened within 5.5 s. While, the

water droplet didn't spread on NC-0.5 (Fig. 7(c)) when it has stayed for 5.5 s, mainly due to their porous microstructures [33]. In the case of the NC-0.75 sample (Fig. 7(d)), there were contact angles which is bigger than right angle, between droplet and carbon surface, for a long observation period. A water contact angle of 97.2°± 1.3° was observed after 15.5 s. In contrast to the above three samples, reduced hydrophilia measured on the NC-0.75 sample could be due to less oxidative functionality and low structural density resulting from the increase of mesopores relative to micropores in the NC-0.75 structure [34]. Furthermore, hysteresis of the electrolyte immersing process in the NC-0.75 sample can be deduced as a result of slight hydrophobicity.

The effect of the obtained carbon materials activated by $NaNO_3$ on the electrochemical performance was investigated by potentiometry study. As presented in Fig. 8(a), cyclic voltammograms (CVs) of the as-prepared samples were carried out in oxygen-saturated 0.1 M KOH solutions at a scan rate of 50 mV s^{-1}. A trend can be observed for the four carbon samples, that the electric double layer areas increased from NC-0 to NC-0.5, and then decreased in NC-0.75, which is in very good agreement with the results of the BET surface areas. Moreover, the CV curves for all as-prepared samples showed obvious redox features, suggesting their catalytic activities for ORR [35]. The pronounced cathodic peaks happened at the following RHE potentials (Fig. 8(b)): NC-0.5 (+0.783 V) > NC-0.75 (+0.782 V) > NC-0.25 (+0.773 V) > NC-0 (+0.748 V), indicating their ORR catalytic ability sequence, which are all much better than our previous work from the same biomass [30]. These results are also superior to or comparable with those carbons reported in the literature

[8, 13, 31].

It has been demonstrated that porous N-doped carbon materials are promising catalysts toward the ORR [21, 36, 37]. The ORR activity of the as-prepared samples was further evaluated by linear sweep voltammetry (LSV) in oxygen-saturated KOH electrolyte (Fig. 8(c)), and benchmarked against state-of-the-art commercial Pt/C. The ORR responses for all the carbon samples presented "S"-shaped curves, similar to that of the Pt/C samples, suggesting high ORR activity of the four carbon materials. The ORR onset potential (corresponding to 0.1 $mA \cdot cm^{-2}$) follows this order: NC-0.25 (+0.952 V) < NC-0.75 (+0.956 V) < NC-0.5 (+0.967 V) < Pt/C (+0.983 V). In addition, as presented in Fig. 8(d), the ORR kinetic current density (j_k) at +0.9 V *vs.* RHE follows this order: NC-0.25 (2.87 mA cm^{-2}_{geo}) < NC-0.75 (3.34 mA cm^{-2}_{geo}) < NC-0.5 (4.19 mA cm^{-2}_{geo}) < Pt/C (4.49 mA cm^{-2}_{geo}). In terms of E_{onset} and j_k, the NC-0.5 sample exhibits comparable ORR activity to that of Pt/C in KOH electrolyte indicating that the NC-0.5 is a promising ORR catalyst. Fig. 8(e) is its LSV curves at different rotation speeds, and inset is the obtained K-L plot at RHE 0.762, compared with ideal 2e and 4e process. As can be seen, the slope is parallel to that of an ideal four-electron procedure. In Fig. 8(f), the current-time curves of NC-0.5 and Pt/C in oxygen saturated 0.1 M KOH were conducted at RHE 0.8 V, with 10 vol% CH_3OH added at the 400th second. The results show that catalyst NC-0.5 isn't active toward the method oxidation reaction [38].

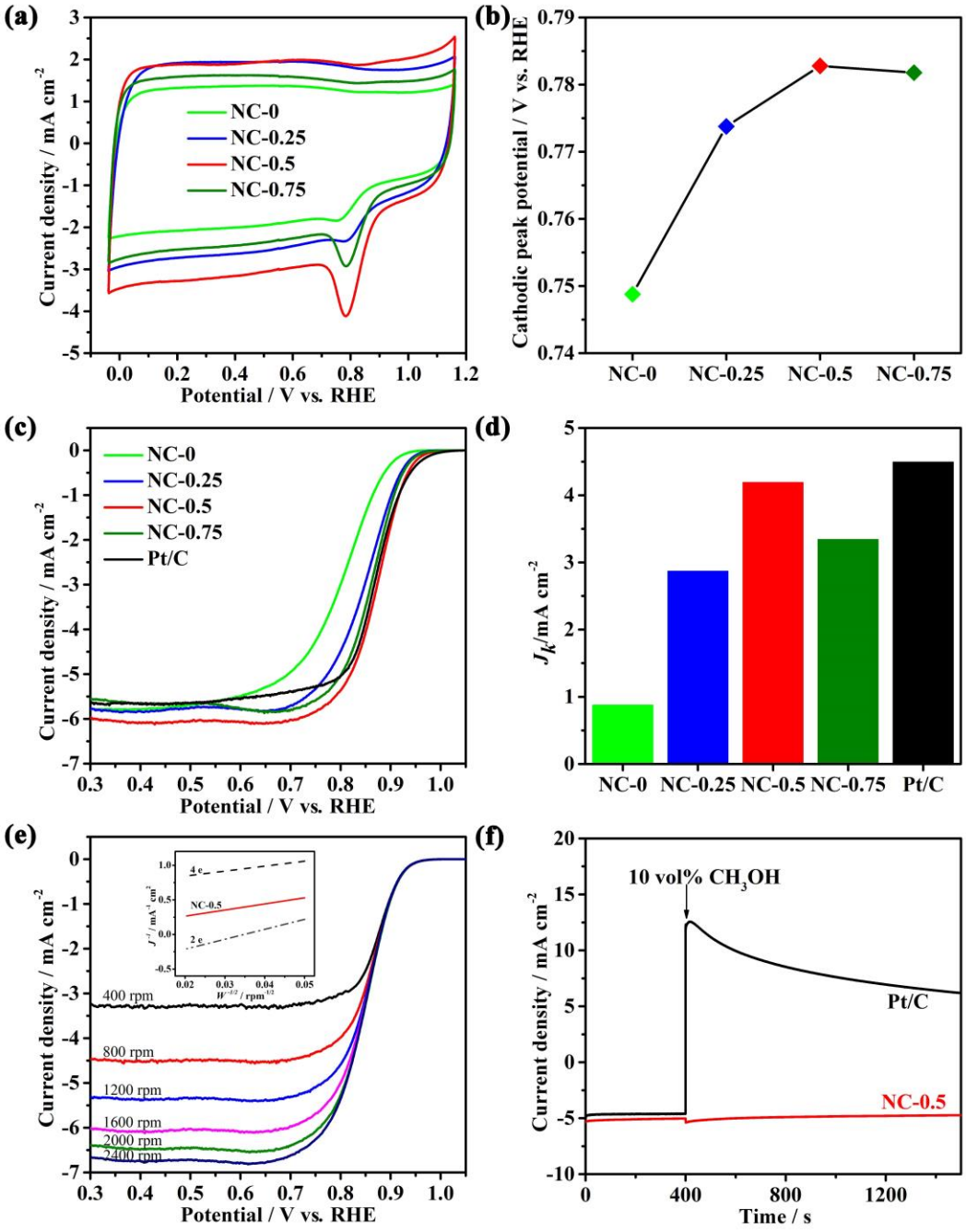

Fig. 8. (a) Cyclic voltammograms and (b) corresponding variation cathodic peaks of NC-0, NC-0.25, NC-0.5 and NC-0.75 materials in oxygen saturated 0.1 M KOH electrolyte at a scan rate of 50 mV s^{-1}. (c) Polarization curves at 1,600 rpm and (d) kinetic currents at + 0.9 V *vs.* RHE for the NC-0, NC-0.25, NC-0.5 and NC-0.75 samples in oxygen-saturated 0.1 M KOH electrolyte at a scan rate of 5 mV s^{-1},

compared to commercial 20 wt% Pt/C. (e) LSV curves of NC-0.5 at different rotation speeds in 0.1 M KOH, inset is the obtained K-L plot at RHE 0.762 V, compared with ideal 2e and 4e process. (f) Current-time curves of NC-0.5 and Pt/C in oxygen saturated 0.1 M KOH at RHE 0.8 V, with 10 vol% CH_3OH added at the 400^{th} second; rotation speed: 1600 rpm.

The variations of the electrochemical performance for the obtained carbon materials could be explained in two-fold as follows: (1) as illustrated in Fig. 9, the structure of the carbon materials becomes more and more open from NC-0 to NC-0.5 based on the SEM and TEM analyses, producing more edges and defects, in turn providing more active sites for the ORR. The formed accessible active surface allowing contact with the electrolyte and the convenience of mass diffusion between the electrolyte and active materials were enhanced, leading to an increase of energy storage capacity and catalytic activity toward the ORR from NC-0 to NC-0.5. On the other hand, the increase in mesopores relative to micropores in the structure of NC-0.75 leads to a low structural density. Then NC-0.75 exhibits slight hydrophobicity (observed from the electrolyte immersing test), resulting in the low storage capacity and catalytic activity toward the ORR compared to NC-0.5. (2) The increase in the content of the graphitic-N and pyridinic-N produces a better ORR performance, whilst the increase in the oxidized N atoms results in a decrease in the hydrophilic property, leading to a decrease in mass transfer, e.g. a reduced electrochemical performance. In a few words, these factors are positive as well as negative in terms of the electrochemical performance for the carbon samples, thus

offering optimal electrochemical performance when the $NaNO_3$ amount is 0.5 g.

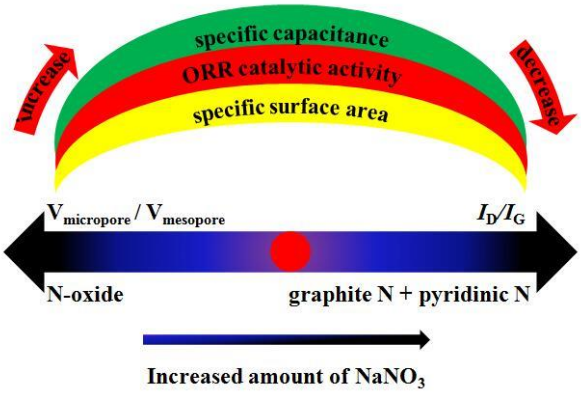

Fig. 9. The diagram of the effect of porous structure and composition on the electrochemical performance of the obtained carbon materials.

4. Conclusions

Hierarchical porous N-doped carbon materials with graphene-like carbon layers derived from soybean dregs (SD) were successfully prepared in a molten salt medium with $NaNO_3$. $NaNO_3$ can act as etching agent to modify the structure of the carbon materials in molten salt medium at high temperatures. Three physical features in carbonized SD can be efficiently tuned by adjusting the amount of $NaNO_3$. Firstly, when the amount of $NaNO_3$ is increased, the structure becomes more and more open, with mesopore ratio increasing from 50.58 % to 90.02 %. Tthe surface area reaches a top value 1430.1 m^2 g^{-1} for NC-0.5. Secondly, the edges and defects increases with an increase of $NaNO_3$, making I_D/I_G value increased from 1.097 to 1.151. Thirdly, the N content increases and the O content decreases as more $NaNO_3$ is added, resulting in longer water droplet infiltration process and even hydrophobic surface of NC-0.5. The chemical state of N atoms also changes which is confirmed by the increase of pyridinic-N and graphitic-N increases and the decrease of pyridinic-N oxide and NO_x

from NC-0 to NC-0.75. Compared to other the as-prepared N-doped carbon, NC-0.5 exhibited the highest catalytic activity toward the oxygen reduction reaction. Moreover, the controllable synthetic strategy reported herein could be extended to the rational design of other opened N-doped carbon nanomaterials of porous structures and high surface areas, which could be promising electrode materials for electrochemical storage devices.

Acknowledgements

The authors would like to thank the National Natural Science Foundation of China (51661008, and 21766032) and Shenzhen Innovation Fund (JCYJ20160520161411353) for financially supporting this work.

References

[1] H. Chen, F. Sun, J. Wang, W. Li, W. Qiao, L. Ling, D. Long, The Journal of Physical Chemistry C, 117 (2013) 8318-8328.
[2] M. Hojamberdiev, R.M. Prasad, K. Morita, M.A. Schiavon, R. Riedel, Microporous and Mesoporous Materials, 151 (2012) 330-338.
[3] N. Fechler, T.P. Fellinger, M. Antonietti, Adv. Mater. , 25 (2013) 75-79.
[4] S. Zhao, T. Yan, H. Wang, J. Zhang, L. Shi, D. Zhang, ACS Applied Materials & Interfaces, 8 (2016) 18027-18035.
[5] C. Zhu, H. Li, S. Fu, D. Du, Y. Lin, Chemical Society Reviews, 45 (2016) 517-531.
[6] M.K. And, M. Jaroniec, R.R. And, H.J. Sang, Journal of Physical Chemistry B, 104 (2000) 7960-7968.
[7] M. Li, F. Xu, H. Li, Y. Wang, Catalysis Science & Technology, 6 (2016) 3670-3693.
[8] R. Wang, T. Zhou, H. Li, H. Wang, H. Feng, J. Goh, S. Ji, Journal of Power Sources, 261 (2014) 238-244.
[9] H. Wang, K. Wang, J. Key, S. Ji, V. Linkov, R. Wang, Journal of the Electrochemical Society, 161 (2014) H637-H642.
[10] H. Duan, T. Yan, G. Chen, J. Zhang, L. Shi, D. Zhang, Chemical Communications, 53 (2017) 7465-7468.
[11] H. Yan, Chemical Communications, 48 (2012) 3430-3432.
[12] W. Kwon, G. Lee, S. Do, T. Joo, S.-W. Rhee, Small, 10 (2014) 506-513.
[13] Y. Zhai, Y. Dou, X. Liu, S.S. Park, C.-S. Ha, D. Zhao, Carbon, 49 (2011) 545-555.
[14] H. Nishihara, T. Kyotani, Advanced Materials, 24 (2012) 4473-4498.
[15] Z. Wang, T. Yan, L. Shi, D. Zhang, ACS Applied Materials & Interfaces, 9 (2017) 15068-15078.

[16] S. Li, R. Xu, H. Wang, D.J.L. Brett, S. Ji, B.G. Pollet, R. Wang, J Solid State Electrochem, (2017) 1-8.
[17] R. Wang, P. Wang, X. Yan, J. Lang, C. Peng, Q. Xue, ACS Appl. Mater. Interfaces 4(2012) 5800-5806.
[18] S. Wei, H. Zhang, Y. Huang, W. Wang, Y. Xia, Z. Yu, Energy Environ. Sci., 4 (2011) 736-740.
[19] J. Kühnle, O. Weis, Surface Science, 340 (1995) 16-22.
[20] T. Ouyang, K. Cheng, Y. Gao, S. Kong, K. Ye, G. Wang, D. Cao, Journal of Materials Chemistry A, 4 (2016) 9832-9843.
[21] R. Wang, H. Song, H. Li, H. Wang, X. Mao, S. Ji, Journal of Power Sources, 278 (2015) 213-217.
[22] M.S. Dresselhaus, A. Jorio, R. Saito, Annual Review of Condensed Matter Physics, 1 (2010) 89-108.
[23] H. Song, H. Li, H. Wang, J. Key, S. Ji, X. Mao, R. Wang, Electrochimica Acta, 147 (2014) 520-526.
[24] Y. Ma, H. Wang, H. Feng, S. Ji, X. Mao, R. Wang, Electrochimica Acta, 142 (2014) 317-323.
[25] S. Brunauer, L.S. Demine, W.E. Deming, E. Teller, J. Am. Chem. Soc., 62 (1940) 1723-1732.
[26] J. Ding, S. Ji, H. Wang, B.G. Pollet, R. Wang, Electrochimica Acta, 255 (2017) 55-62.
[27] Y. Chen, H. Wang, S. Ji, R. Wang, Catalysis Communications, 107 (2018) 29-32.
[28] R. Arrigo, M. Havecker, R. Schlogl, D.S. Su, Chemical Communications, (2008) 4891-4893.
[29] G.A. Ferrero, K. Preuss, A.B. Fuertes, M. Sevilla, M.M. Titirici, J. Mater. Chem. A, 4 (2016) 2581-2589.
[30] R. Wang, H. Wang, T. Zhou, J. Key, Y. Ma, Z. Zhang, Q. Wang, S. Ji, Journal of Power Sources, 274 (2015) 741-747.
[31] R. Liu, D. Wu, X. Feng, K. Müllen, Angewandte Chemie International Edition, 49 (2010) 2565-2569.
[32] J. Li, D. Li, Y. Yang, J. Li, F. Zha, Z. Lei, Green Chemistry, 18 (2016) 541-549.
[33] X. Liu, C. Giordano, M. Antonietti, Small, 10 (2014) 193-200.
[34] C.-H. Huang, C.-Y. Su, C.-S. Lai, Y.-C. Li, S. Samukawa, Carbon, 73 (2014) 244-251.
[35] Y. Chen, S. Huo, H. Wang, Micro & Nano Letters, Institution of Engineering and Technology, 2018.
[36] R. Wang, K. Wang, Z. Wang, H. Song, H. Wang, S. Ji, Journal of Power Sources, 297 (2015) 295-301.
[37] G. Wu, Z. Chen, K. Artyushkova, F.H. Garzon, P. Zelenay, ECS Trans., 16 (2008) 159-170.
[38] W. Yuan, Y. Feng, A. Xie, X. Zhang, F. Huang, S. Li, X. Zhang, Y. Shen, Nanoscale, 8 (2016) 8704-8711.